Fatigue assessment of as-built and heat-treated Inconel 718 specimens produced by additive manufacturing including notch effects

Klas Solberg[a,*], Di Wan[a], Filippo Berto[a]

[a]*Department of Mechanical and Industrial Engineering, Norwegian University of Science and Technology, 7034 Trondheim, Norway*

Abstract

The fatigue behaviour of notched and unnotched specimens produced by additively manufactured Inconel 718 are analysed in the as-built and heat-treated conditions. The surfaces display high roughness and defects acting as fatigue initiation sites. In the as-built condition, fine sub-grains were found, while in the heat-treated state, the sub-grains were removed and the dislocation density recovered. SN-curves are predicted based on tensile properties, hardness and defects obtained by fractography, using the $\sqrt{\text{area}}$-method.

Keywords:
Fatigue, Additive manufacturing, Heat treatment, Inconel 718, Defects, Selective laser melting

1. Introduction

Additive Manufacturing (AM) is a fast-rising production method allowing components to be produced by adding material rather than forming or subtracting, as is characteristic for many established conventional processes. Many design restrictions are avoided with AM and parts can be manufactured with a high degree of design freedom. However, some challenges also arise with the new manufacturing method: high surface roughness, anisotropic microstructure, porosity and residual stresses.[1,2,3] Due to this, the fatigue behaviour of the materials are often reduced compared to the wrought condition. In particular, the geometric defects such as porosity, surface roughness and lack of fusion reduce the fatigue

*Corresponding author
Email address: klas.solberg@ntnu.no (Klas Solberg)

strengths.[4,5,6,7] The defects in the surface region can be removed by machining, and internal pores can be closed by hot isostatic pressing. In many cases, machining is not possible due to the desired complexity of the designed components. However, heat treatments might still be possible to improve the fatigue performance. This is particularly true for alloys such as Inconel 718, whose performance is strongly correlated to the heat treatment schemes.

Inconel 718 is a precipitation hardening alloy which displays high yield, tensile, creep and fatigue strengths at temperatures up to 700°C. In addition to this, the alloy has high weldability, making it a good candidate for AM. The alloy is commonly used in the aerospace, and the oil and gas industry, employing different heat treatment schemes for various applications.[8] There are several possible heat treatment schemes for Inconel 718, and they usually consist of two main stages: (i) homogenization and/or solution treatment at 980-1200°C for dissolving hardening constituents into the matrix and (ii) Ageing treatment at 650-900°C for forming γ' and γ'' precipitates. The ageing process is usually done in two steps.

Due to the high temperature gradients in AM processes such as Selective Laser Melting (SLM), the microstructure usually shows different features than those produced by conventional manufacturing. Typically fine subgrain/dendritic structures are observed in the as-built state.[9] As a result of this, researchers are working on tailoring heat treatments for AM applications.[9,10]

Dealing with fatigue, the general conclusion is that the material is sensitive to defects. The material displays its lowest fatigue strength in the as-built condition, where the surface roughness tends to be high. However, the scatter in fatigue life tends to be low. The reason for the low scatter is the AB surface which causes premature failure. When machined, the fatigue strength of the material is increased.[11] Here, defects may be present as internal porosity or lack-of-fusion. Their locations and distributions usually cause a higher scatter in the fatigue data.[11] In terms of anisotropy, the specimens manufactured horizontally displays longer fatigue life than those manufactured vertically.[1,12,13] Hot isostatic pressing can close internal porosity and has been reported to increase the fatigue strength to the same level as wrought,[14] however, it has also been reported to reduce the strength due to microstructural effects.[15]

In this work, the fatigue behaviour of AM Inconel 718 are investigated in the as-built(AB) and the heat-treated (HT) state. This was done for both notched and unnotched specimens. The microstructures of the two different material states were investigated and compared. Defects from the fracture surfaces were captured, and the hardness of the two materials were

measured. SN-curves of the different materials and geometries were predicted based on the tensile properties and the $\sqrt{\text{area}}$-method[16] using hardness and defect sizes.

It should be noted that this work is a continuation of a previous work where the fatigue behaviour was studied in the AB condition,[17] the same specimen geometries and process parameters have been used.

2. material and methods

In the present work, Inconel 718 specimens produced by SLM are studied. The chemical composition of the material is defined in Table. 1 as per ASTM F3055-14a. Three different specimen geometries were considered: one specimen geometry for static loading; two specimen geometries for fatigue loading. The geometries are shown in Fig. 1. The specimen for quasi-static loading was designed according to ASTM E8. The two geometries for fatigue loading were the same as the ones employed in;[17] One unnotched and one double v-notch geometry. The specimens were built with a layer height of 50 μm and an energy density of 60 J/mm^3.

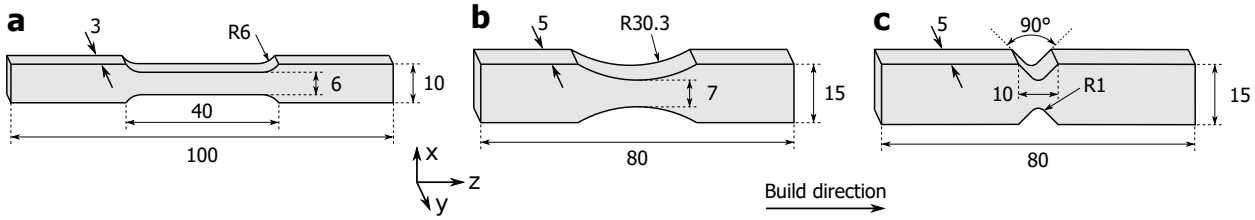

Figure 1: Dimensions of specimens: **(a)** tensile specimen, thickness 3 mm; **(b)** Unnotched fatigue specimen, thickness 5 mm; **(c)** Notched fatigue specimens, thickness 5 mm. All specimens are built in z-direction.

Ni	Fe	Cr	Nb	Mo	Ti	Al	Co	Si	Mn	Cu
50-55	11-22.4	17-21	4.8-5.5	2.8-3.3	0.7-1.2	0.2-0.8	1.0	0.4	0.4	0.3

Table 1: Chemical composition of Inconel 718 as defined by ASTM in wt% [REF ASTM]

The specimens were tested in two different conditions: as-built and heat-treated. The specimens were heat-treated at 1095 °C for 1 h then air-cooled to room temperature and double aged 720 °C for 8 h furnace cooled 50 °C/h and treated at 620 °C for 8 h and air-cooled to room temperature.

Mechanical loading was done using a servohydraulic MTS uniaxial testing system with a load cell of 50 kN. The fatigue testing was done using the same system, a loading ratio $R = 0$ and a frequency of 10 Hz was used. Vickers hardness measurements were done on a Mitutoyo MicroWiZhard system; the reported values were taken as the average and standard deviation of ten measurements in each orientation.

Fractography was done using a Quanta FEG 650 Scanning Electron Microscope (SEM). The microstructure was analysed by different approaches. Analysis done by optical microscope was done by polishing cross-sections and Kalling's reagent according to ASTM E407-07. The final stage of polishing was 1 μm diamond paste. For Electron BackScatter Diffraction (EBSD) and BackScattered-Electron (BSE) analysis, the specimens were not etched but prepared by oxide polishing suspensions, with a particle size of 0.25 μm.

3. Results

3.1. Mechanical behaviour and fatigue data

Based on the tensile tests, the AB specimen showed a tensile strength of 948 MPa and an elongation of 13.0 %. After heat treatment, a tensile strength of 1374 MPa and an elongation of 7.7% was achieved. The increase in strength and reduction in elongation is typical when heat treating AM Inconel 718.[1,18] However, the results obtained here show somewhat lower elongation the other data in the literature.[1] The low elongation in both cases can be attributed to the fact that the specimens were tested with the as-built surface. A strong correlation between the surface roughness and elongation at failure for Ti6Al4V was recently demonstrated by Barba *et al.*[19]

Hardness measurements of the AB and HT materials were done in the xy- and xz-planes, referring to the coordinate system in Fig. 1. The results are shown in Table 2, and shows that for AB the hardness was ∼300 HV and for HT the hardness was ∼500 HV.

AB xy	AB xz	HT xy	HT xz
314.1 ± 16.2	311.1 ± 14.1	494.5 ± 19.0	512.9 ± 19.4

Table 2: Vickers hardness measurements of AB and HT specimens in xy- and xz-planes.

The fatigue data are collected in the SN-diagram in Fig. 2. Both for unnotched and notched specimens, the fatigue strength is increased when comparing HT to AB. Basquin

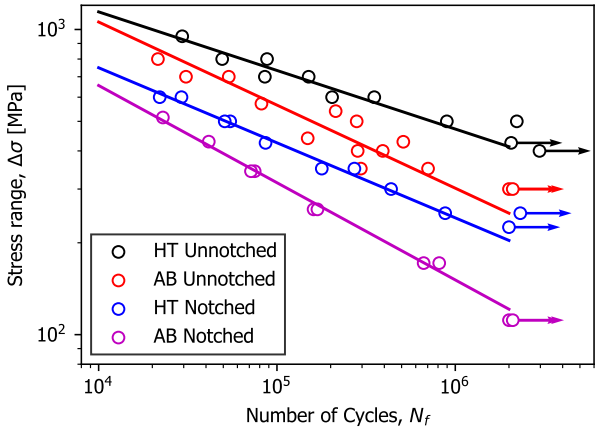

Figure 2: Fatigue data of HT and AB specimens. Tests were performed with a loading ratio R=0 and frequency of 10 Hz.

	$\Delta\sigma$	k
HT Unnotched	420.5	5.21
AB Unnotched	250.0	3.67
HT Notched	203.2	4.07
AB Notched	121.2	3.14

Table 3: Summary of the fatigue strength, $\Delta\sigma$, at 2×10^6 cycles and the inverse slope, k, of the regression lines in Fig. 2.

law regression lines were added in the range of 10^4 and 2×10^6 cycles, the fatigue strength at 2×10^6 cycles and the inverse slope of the curves are shown in Table 3.

3.2. Fractographies

Fracture surfaces of the four different specimen categories are shown in Fig. 3a-d. In the unnotched specimens, the same trend is observed for AB and HT; fatigue initiates from a local defect in the surface and propagates towards the other side of the specimen (indicated by the arrows). For the notched specimens, two different fracture processes are observed; crack propagation from both notches (Fig. 3c) and crack propagation from one notch(in Fig. 3d). The AB specimens experienced crack propagation from both notches, while for the HT specimens had both cases.

The size and morphology of the defects initiating fatigue are shown in Fig. 3e-h. No distinct difference in the defect morphologies are observed when comparing the AB specimens

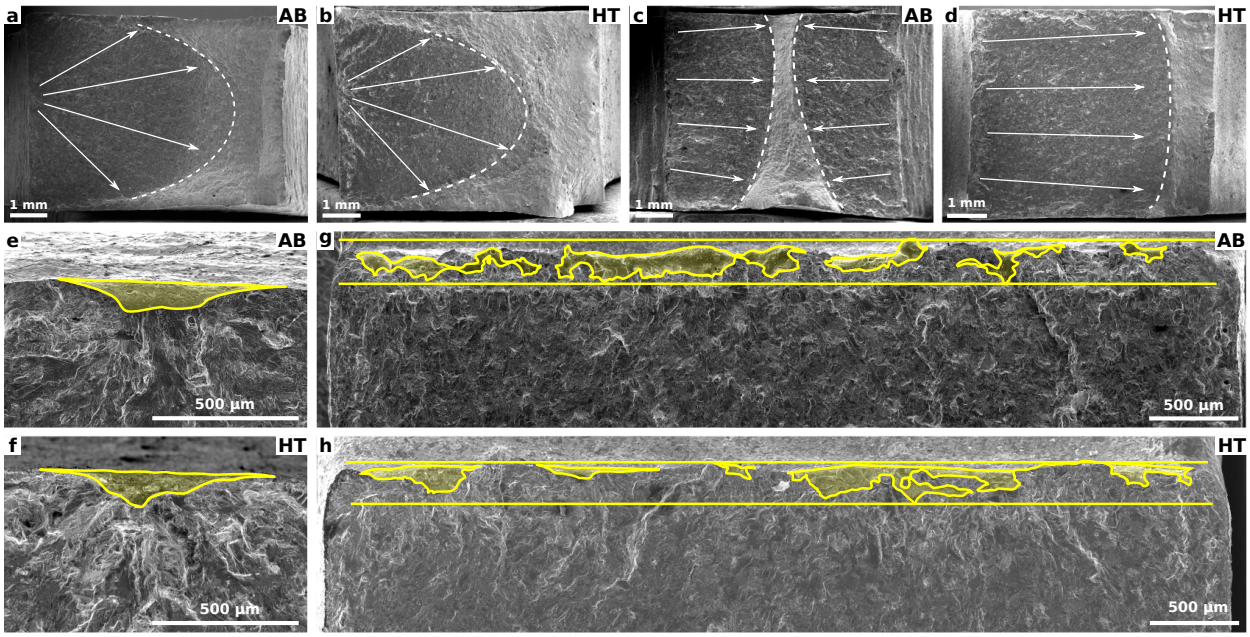

Figure 3: Fracture surface and detail of defects initiating fatigue of the different specimen types: (a-b) unnotched, overview; (c-d) notched, overview; (e-f) unnotched, initiation; (g-h) notched, initiation. 3The material conditions are marked in each sub-figure.

to the HT specimens; the unnotched specimens fail from local defects, while the notched specimens fail from defects distributed along the thickness direction of the sample.

3.3. Failure locations and surface defects

The cross-sections of one AB and one HT notched specimen subjected to 2×10^6 cycles of loading are compared in Fig. 4. The same general trends are observed: defect populated down-skin region and smoother up-skin surface. The AB specimen displays fatigue crack initiation from the down-skin region; this is not observed within the HT specimen. It should be noted that the morphology of the defects adjacent to the notch root is not the same. Further, Fig. 4 evaluates one plane within the material, which is not necessarily representable for the whole cross-section.

According to recent research, notch geometries produced by AM subjected to fatigue loading does not necessarily fail from the designed notches, but rather from defects related to the manufacturing process, dependent on the notch acuity and the size of the defects.[17,20] Both the AB and HT specimens display the same general surface morphology and similar values of Rz can be assumed: 77 μm and 259 μm for the up-skin and down-skin respectively.[21] It should be noted that an oxide film was formed on the surface in the HT specimens, as

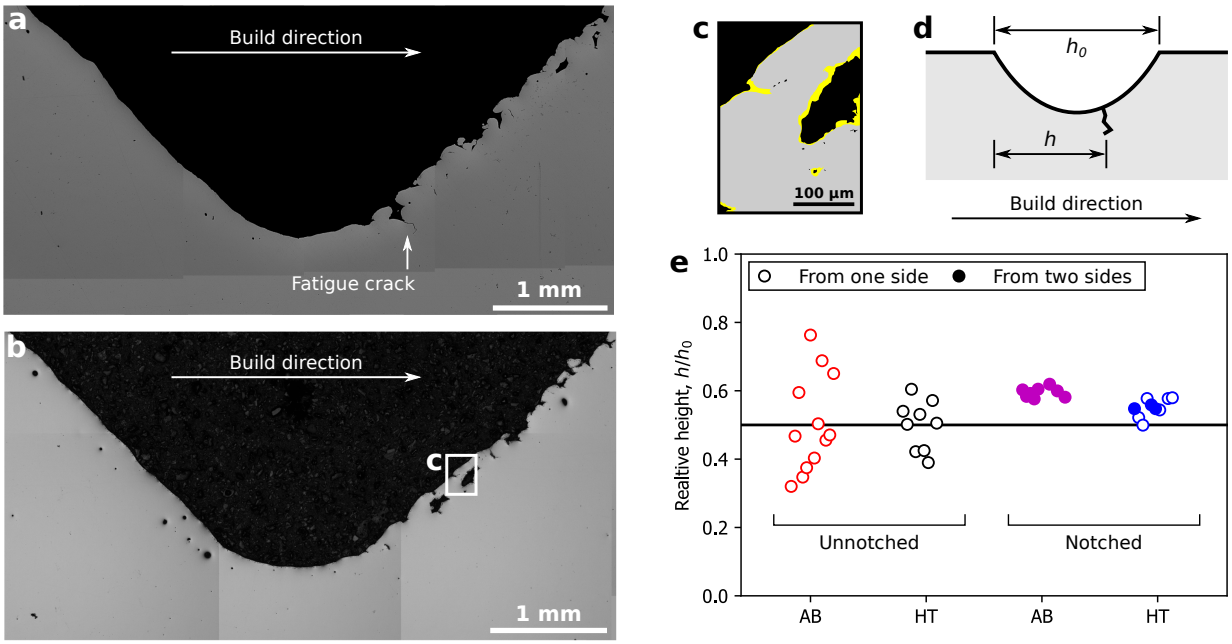

Figure 4: Polished cross sections of notched specimens subjected to 2×10^6 cycles: (a) AB and (b) HT. (c) highlighted oxide layer (yellow). (d) Definition of failure site: relative height, h/h_0 (e) Failure locations for the various tests

highlighted in Fig. 4e.

The trends in failure locations are shown in Fig. 4. For the unnotched specimens, AB displays a high scatter in failure locations compared to HT. Based on these differences, it seems like the AB specimens are less sensitive to the nominal stress level, and more sensitive to defects than HT. Further, some differences are observed when comparing the notched specimens. For AB specimens, fatigue initiated from both sides, and always in the down-skin region. For the HT specimens, fatigue shifted between failure from one or two sides. In addition to this, some specimens failed from closer to the notch root.

3.4. Microstructure

The microstructure of the AB and HT condition are shown in Fig. 5a and b, respectively. In AB, the hatch pattern and melt pool morphologies are visible, elongated grains are observed in the build direction (xz- and yz-planes) and equiaxed grains in the xy-plane. In the case of HT, the same general trends are observed. However, the hatching pattern and melt pool morphologies are not as visible. The general microstructure is typical for Inconel 718 produced by SLM.[1] The two different materials were further analysed by EBSD; this analysis is shown in Fig. 6.

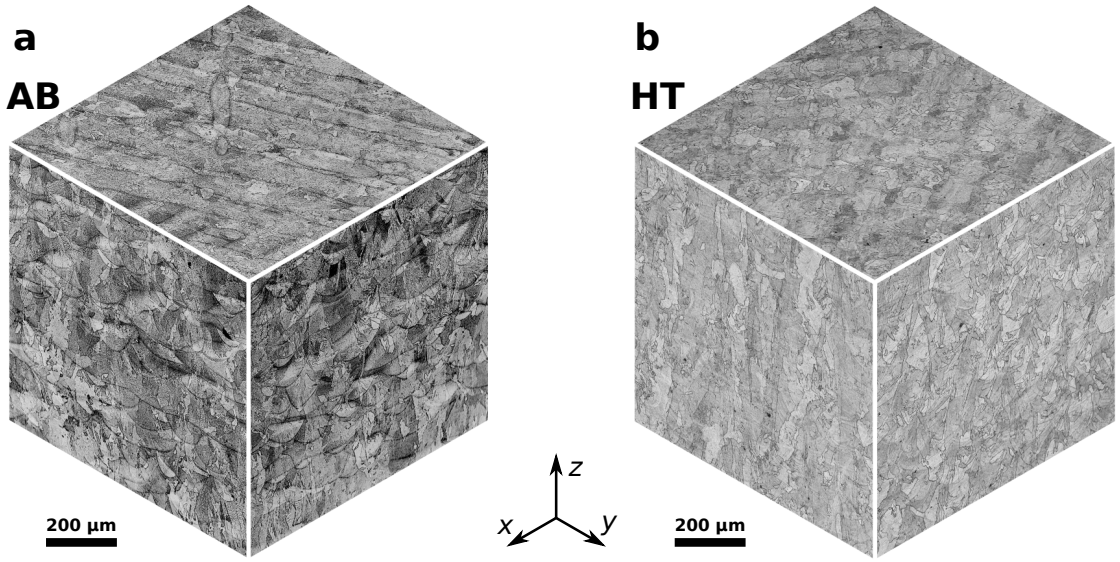

Figure 5: Comparison of the general microstructure and the surface conditions in AB and HT (a) 3 planes of microstructure in AB, (b) 3 planes of microstructure in HT.

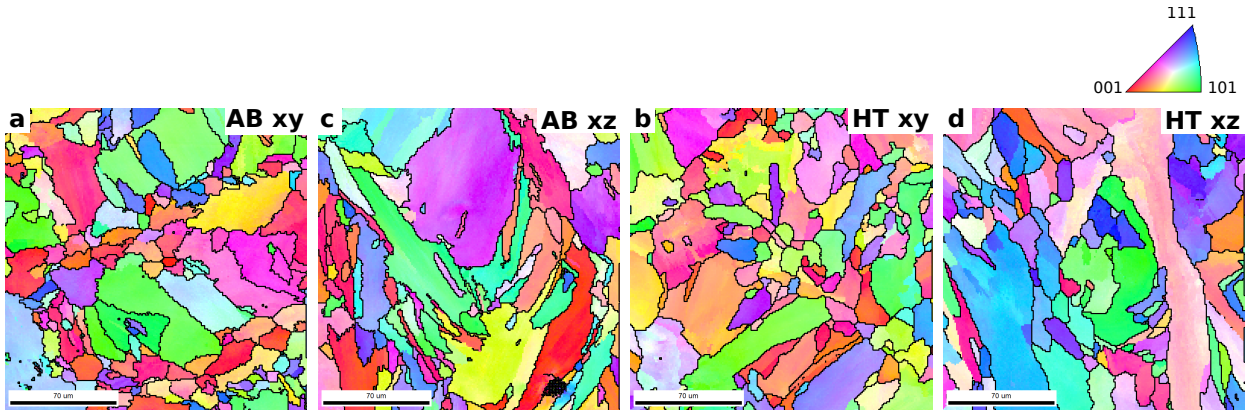

Figure 6: General microstructure obtained by EBSD in terms of normal direction -inverse pole figure (ND-IPF) maps. (a) AB xy-plane, (b) HT xy-plane, (c) AB xz-plane and (d) HT xz-plane. The coloring criterion is the same for all sub-figures, shown by the IPF in the upper right corner.

The structure of the grains are shown in Fig. 7. Fig. 7a and d show the difference between AB and HT in the xz-plane. In the AB condition, a refined sub-grain structure is observed; in the HT specimen, the boundaries seem erased/smoothed compared to AB. The same trends are observed in the xy-plane, in Fig. 7b and e. In the case of AB, the sub-grains show the same trend as the general microstructure; elongated in the build direction and equiaxed in the xy-plane. Further, precipitates are observed at the grain boundaries in the HT specimen, as indicated by arrows in Fig. 7d. Further, the dislocation density is

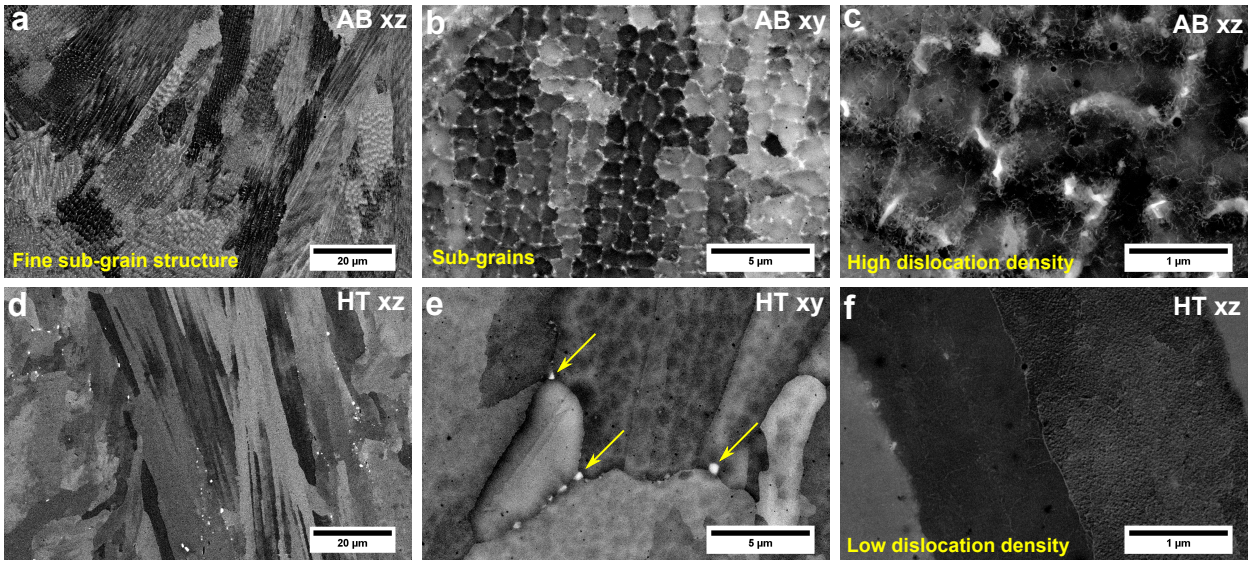

Figure 7: SEM analysis of the microstructure of AB (a,c,e) and HT (b,d,f) material. (a) xz-plane, (b) xz-plane (c) xy (d) xy (e) xz high dislocation density visible (f) xz, low dislocation density visible.

compared in Fig. 7c and f. The white lines indicate the dislocations. A reduced dislocation density is observed when comparing HT to AB, the same was observed by Zhang *et al.*[18]

3.5. Fatigue life predictions

When designing against fatigue, SN-diagrams are frequently used to determine the critical load levels. For design purposes, SN-diagrams can either be developed based on experimental data or they can be estimated. In this section, we demonstrate how the Murakami-method[16] and the tensile behaviour can be used for estimating SN-diagrams for AM metals.

The Murakami-model has been frequently employed when analysing AM metals.[22,4,23] The model predicts the fatigue limit, σ_w, based on the hardness and the defect size, $\sqrt{\text{area}}$. The fatigue limit can be estimated (for R=-1 loading) by the following relation:

$$\sigma_{w,R=-1} = \frac{1.43(Hv + 120)}{(\sqrt{area})^{1/6}}. \quad (1)$$

In order to predict the fatigue behaviour the following assumptions were made:

1. The fatigue strength can be predicted to be equal to the tensile strength, σ_{uts}, at $\sim 10^3$ cycles. This is a good estimate for many ductile engineering materials at R=0.[24] This is can also be used for notched specimens due to the notch strengthening effect.[21]

2. The fatigue limit can be predicted based on the critical defect size and the hardness employing the $\sqrt{\text{area}}$-method by Murakami. Note that the fatigue limit should also be corrected for the mean stress and the stress concentration.
3. The slope of the SN-diagram can be estimated based on the two above-mentioned estimates by the Basquin law.

In the case of the fatigue data presented here, the defect-sizes were measured for all the AB specimens. Based on the micrograph in Fig. 4a and b, there are no differences in the surface morphology of AB and HT specimens. This indicates that the defects obtained in the AB specimens can be used to predict the fatigue life of the HT specimens. The loading ratio for the fatigue data in this work is R=0; this means that a mean stress correction should be made of the Murakami-model. The SWT mean stress correction was used.[25] The SWT mean stress correction is given by

$$\sigma_{ar} = \sigma_a \sqrt{\frac{2}{1-R}}, \tag{2}$$

where σ_a is the stress amplitude and σ_{ar} is the equivalent stress amplitude for R=-1. The fatigue limit expressed in terms of the stress range corrected to R=0 loading can then be expressed as

$$\Delta\sigma_{w,R=0} = \sqrt{2} \cdot \frac{1.43(Hv + 120)}{(\sqrt{area})^{1/6}}. \tag{3}$$

The $\sqrt{\text{area}}$ should be taken as the effective defect area projected onto the plane perpendicular to the loading direction. Both in the case of unnotched and notched specimens, the largest defect obtained from fractography was used. The defects and the estimated effective area are shown in Fig. 8. In the case of the unnotched specimen, a semi ellipse was drawn around the defect. In the case of the notched specimens, defects were present along the edge of the notch, and in this case, the effective defect size was taken to be $10c$, where c is the maximum depth of the defect (as suggested in by Murakami[26]). Based on these assumptions, the predicted fatigue life curves are shown in Fig. 9a, and the accuracy of the predictions are shown in Fig. 9b.

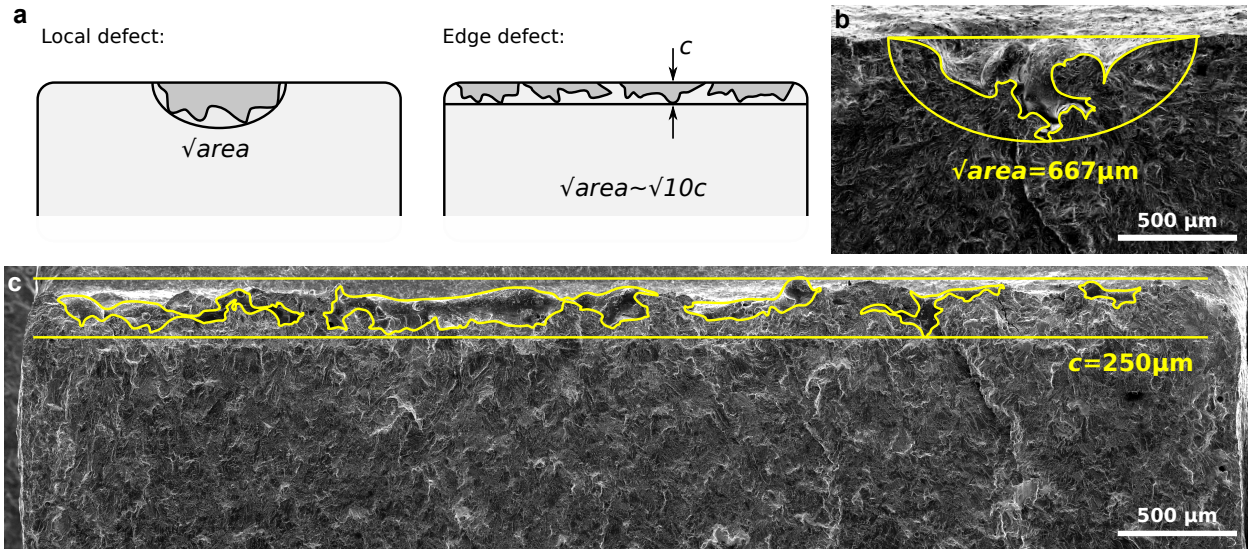

Figure 8: Defects and effective defect area of (a) unnotched specimen and (b) v-notched specimen. (c) Method of estimating the effective defect area of local and edge defects

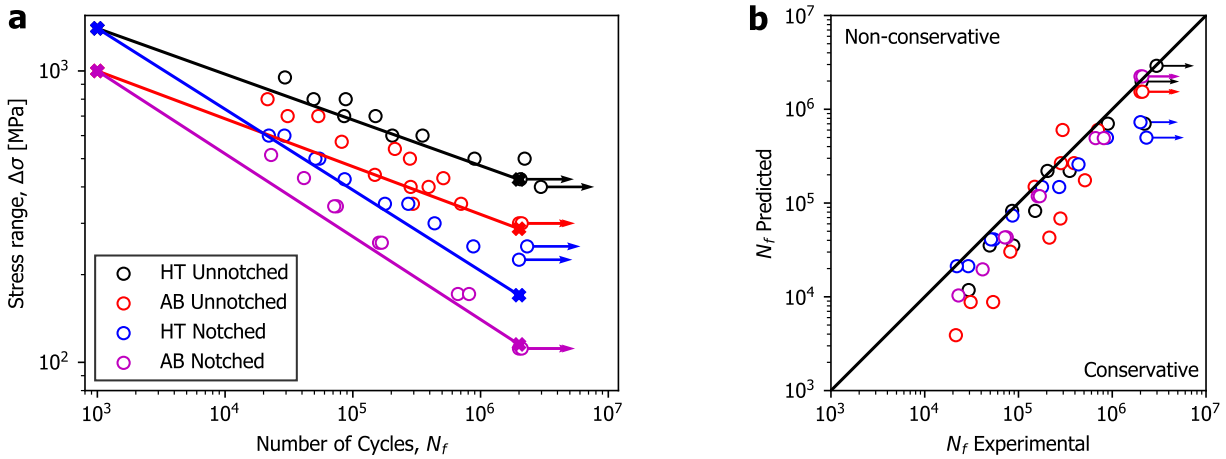

Figure 9: (a) Fatigue life curves predicted based on Murakami-method and tensile properties. (b) Accuracy of SN-curve predictions

4. Discussion

4.1. Failure locations

In Fig. 4, changes in failure locations are observed when comparing AB and HT. Several explanations can be used for describing the change in failure locations observed when comparing the AB and HT specimens.

The first explanation is based on the ideas of Wan *et al.*, where they proposed that

heat treatment of AM Inconel 718 could increase the resistance to fatigue initiation.[10] This would be equivalent to altering the *critical distance* of the material.[27] The idea of the critical distance derived from Neuber,[28,29] who proposed that failure is initiating when the stress at a critical distance (or along a structural support length) away from the surface reaches a critical value.[30] This explanation would indicate that the heat treatment was able to alter the critical distance, making the stress from the notch root more critical than the stress from the defects. Usually, the critical distance is lower for high strength materials, making them more sensitive to defects. However, if heat treatments can increase the strength while also increasing the critical distance, it would be a huge benefit in AM applications.

Another explanation could be the effect of the oxide film. The oxide film in HT specimen can be observed in Fig. 4c. The oxide film forms on any free surface and might have a similar effect to what has been observed in high-temperature fatigue of Inconel 718. In high-temperature fatigue of Inconel 718, some researchers are attributing the high fatigue strength and the retardation of short crack growth to the formation of oxide films at the crack tip, which suppresses slipping.[31] Assuming that the as-built surfaces are "pre-cracked" due to the defects in the surface region, the initiation of crack growth might be suppressed by the oxide film. In addition to this, the oxide films could be "blunting" the defects, so that an oxide layer covers their initial sharp radius. If oxide films can increase the fatigue limits in AM components, it would be a straightforward and cheap way to do the post-processing. In conventional components, the oxide film might change the appearance or the tolerances, while in AM the surfaces are rough, and it would not matter if an oxide film is present or not if the as-built surface is used.

A third explanation could be a statistical difference in the defects of the AB and HT specimens. From Fig. 4, it seems that the same morphologies of defects are present in the down-skin region for both specimens. From the fractographies in Fig. 3, defects of similar sizes and morphologies were found in the AB and HT specimens.

4.2. The $\sqrt{area}$-method

The modified approach of the Murakami-method proposed here can give predictions of the fatigue strengths of both notched and unnotched specimens based on tensile properties, hardness and defect-size. The estimates give conservative predictions; however, this result is dependent on what number of cycles one states the fatigue limit to be at. *E.g.* if the fatigue limit is stated to be at 10^7 cycles, then the predictions would be less conservative.

It should also be noted that many effects are not taken into account, such as residual stresses and microstructural anisotropy. Despite this, the model can be useful when designing components.

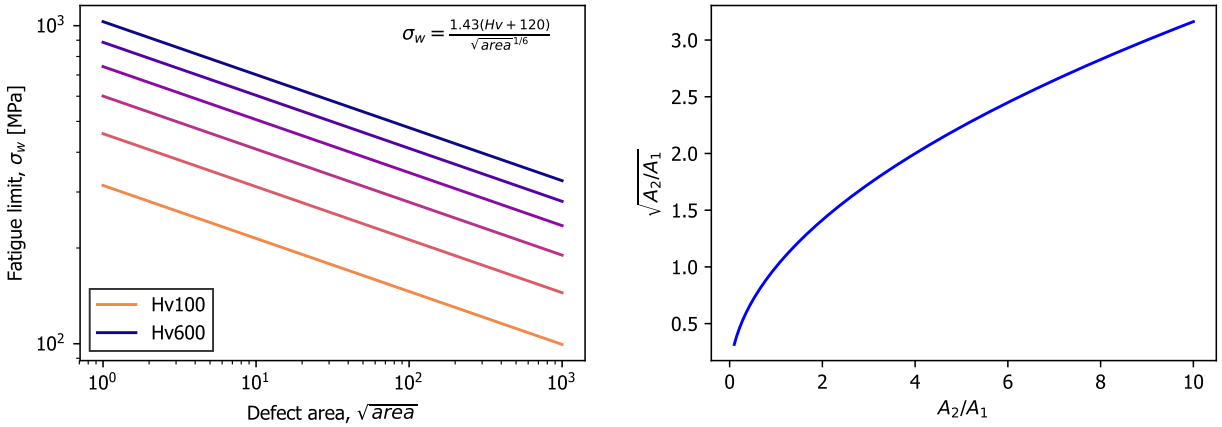

Figure 10: (a) The effect of Hv and $\sqrt{\text{area}}$ on the fatigue limit predicted by Murakami. (b) The influence of the area measured.

One of the main issues dealing with the $\sqrt{\text{area}}$ method is that the effective defect area should be used. In order to obtain this area, specimens usually need to be broken in the HCF-regime. But how much does the accuracy of the parameter matter on the fatigue limit predictions? There is a linear relationship between the hardness and the fatigue limit, while there is an exponential relation between the defect size and the fatigue limit. In Fig. 10a, the fatigue limit predictions are plotted versus $\sqrt{\text{area}}$ for Hv values ranging from 100 to 600.

The defect range in AM is typically one order of magnitude, *e.g.* $10^1 - 10^2$ μm. Due to this, making a mistake in calculation, *e.g.* 50% will have a very small impact on the result. The Murakami model is only concerned with the order of magnitude of the defect.

The measurement of the effective area in the Murakami model leaves room for deviations. The plot in Fig. 10b shows the effect of deviating measurements. If A_2 is overestimated, e.g. by a factor of 10, the resulting error in $\sqrt{}$ is only by a factor of 3. If A_2 is underestimated by a factor 0.1, the resulting error in $\sqrt{}$ is by a factor of 0.3. This means that by taking $\sqrt{\text{area}}$, the errors are corrected to be closer to the real area.

5. Conclusions

Additively manufactured Inconel 718 was analysed in the AB and HT state. The tensile and fatigue behaviour of the material were evaluated. Further, the Murakami-model was employed for predicting SN-diagrams. The following conclusions can be drawn:

- Heat treatment of as-built specimens increased the tensile strength, the hardness, and the fatigue strength and decreased the elongation.
- The microstructure showed typical columnar grains in the build direction for both AB and HT. In the AB state, fine subgrain structures were observed; these were erased after HT and precipitates were observed at the grain boundaries. The dislocation density was reduced after heat treatment.
- SN-curves were predicted based on the Murakami-model and the tensile strengths, for both unnotched and notched specimens. The predictions indicated that the method is suitable design purposes in engineering applications.
- By analysing the failure locations in the AB and HT specimens, it was observed that, although the surface morphologies were the same, the failure locations were shifted. This result shows that by analysing the statistics of the failure locations, it is possible to state that the material has a different sensitivity to the surface roughness in the HT state.

Acknowledgement

The authors would like to acknowledge Marius Hornnes for experimental works associated with his master's thesis.

CRediT authorship contribution statement

Klas Solberg: Conceptualization, Formal analysis, Investigation, Visualization, Writing - Original Draft **Di Wan**: Investigation, Writing - Review & Editing **Filippo Berto**: Conceptualization, Writing - Review & Editing, Supervision

References

[1] E. Hosseini, V. Popovich, A review of mechanical properties of additively manufactured inconel 718, Additive Manufacturing 30 (2019) 100877.

[2] G. Vastola, G. Zhang, Q. Pei, Y.-W. Zhang, Controlling of residual stress in additive manufacturing of ti6al4v by finite element modeling, Additive Manufacturing 12 (2016) 231 – 239.

[3] M. Megahed, H.-W. Mindt, N. NDri, H. Duan, O. Desmaison, Metal additive-manufacturing process and residual stress modeling, Integrating Materials and Manufacturing Innovation 5 (2016) 6193.

[4] S. Tammas-Williams, P. Withers, I. Todd, P. Prangnell, The influence of porosity on fatigue crack initiation in additively manufactured titanium components, Scientific Reports 7 (2017) 7308.

[5] P. Li, D. Warner, A. Fatemi, N. Phan, Critical assessment of the fatigue performance of additively manufactured ti6al4v and perspective for future research, International Journal of Fatigue 85 (2016) 130 – 143.

[6] R. Molaei, A. Fatemi, N. Phan, Significance of hot isostatic pressing (hip) on multiaxial deformation and fatigue behaviors of additive manufactured ti-6al-4v including build orientation and surface roughness effects, International Journal of Fatigue 7 (2018) 352 – 370.

[7] A. Yadollahi, N. Shamsaei, Additive manufacturing of fatigue resistant materials: Challenges and opportunities, International Journal of Fatigue 98 (2017) 14 – 31.

[8] M. J. Donachie, S. J. Donachie, Superalloys, a techinal guide, ASM International.

[9] W. M. Tucho, P. Cuvillier, A. Sjolyst-Kverneland, V. Hansen, Microstructure and hardness studies of inconel 718 manufactured by selective laser melting before and after solution heat treatment, Materials Science and Engineering: A 689 (2017) 220 – 232.

[10] H.-Y. Wan, Z.-J. Zhou, C.-P. Li, G.-F. Chen, G.-P. Zhang, Enhancing fatigue strength of selective laser melting-fabricated inconel 718 by tailoring heat treatment route, Advanced Engineering Materials 20 (10) (2018) 1800307.

[11] A. R. Balachandramurthi, J. Moverare, N. Dixit, R. Pederson, Influence of defects and as-built surface roughness on fatigue properties of additively manufactured alloy 718, Materials Science and Engineering: A 735 (2018) 463 – 474.

[12] R. Konen, G. Nicoletto, L. Kunz, A. Baa, Microstructure and directional fatigue behavior of inconel 718 produced by selective laser melting, Procedia Structural Integrity 2 (2016) 2381 – 2388.

[13] P. F. Kelley, Fatigue behavior of direct metal laser sintered (dmls) inconel 718, MSc thesis, Tufts University (2016).

[14] D. B. Witkin, D. Patel, T. V. Albright, G. E. Bean, T. McLouth, Influence of surface conditions and specimen orientation on high cycle fatigue properties of inconel 718 prepared by laser powder bed fusion, International Journal of Fatigue 132 (2020) 105392.

[15] M. Aydinoz, F. Brenne, M. Schaper, C. Schaak, W. Tillmann, J. Nellesen, T. Niendorf, On the microstructural and mechanical properties of post-treated additively manufactured inconel 718 superalloy under quasi-static and cyclic loading, Materials Science and Engineering: A 669 (2016) 246 – 258.

[16] Y. Murakami, Chapter 5 - effect of hardness hv on fatigue limits of materials containing defects, and fatigue limit prediction equations, in: Y. Murakami (Ed.), Metal Fatigue, Elsevier Science Ltd, Oxford,

2002, pp. 57 – 74.

[17] K. Solberg, F. Berto, Notch-defect interaction in additively manufactured inconel 718, International Journal of Fatigue 122 (2019) 35 – 45.

[18] D. Zhang, W. Niu, X. Cao, Z. Liu, Effect of standard heat treatment on the microstructure and mechanical properties of selective laser melting manufactured inconel 718 superalloy, Materials Science and Engineering: A 644 (2015) 32 – 40.

[19] D. Barba, C. Alabort, Y. Tang, M. Viscasillas, R. Reed, E. Alabort, On the size and orientation effect in additive manufactured ti-6al-4v, Materials & Design 186 (2020) 108235.

[20] K. Solberg, F. Berto, A diagram for capturing and predicting failure locations in notch geometries produced by additive manufacturing, International Journal of Fatigue 134 (2020) 105428.

[21] K. Solberg, F. Berto, The effect of defects and notches in quasi-static and fatigue loading of inconel 718 specimens produced by selective laser melting, International Journal of Fatigue (In press).

[22] Y. Yamashita, T. Murakami, R. Mihara, M. Okada, Y. Murakami, Defect analysis and fatigue design basis for ni-based superalloy 718 manufactured by selective laser melting, International Journal of Fatigue 117 (2018) 485 – 495.

[23] J. Gunther, D. Krewerth, T. Lippmann, S. Leuders, T. Troster, A. Weidner, H. Biermann, T. Niendorf, Fatigue life of additively manufactured ti6al4v in the very high cycle fatigue regime, International Journal of Fatigue 94 (2017) 236 – 245, fatigue and Fracture Behavior of Additive Manufactured Parts.

[24] N. E. Dowling, Mechanical behavior of materials, 4th edition, Pearson.

[25] K. Smith, T. Topper, P. Watson, A stress - strain function for the fatigue of metals, Journal of Materials 5 (1970) 767–778.

[26] Y. Murakami, Chapter 2 - stress concentration, in: Y. Murakami (Ed.), Metal Fatigue, Elsevier Science Ltd, Oxford, 2002, pp. 11 – 24.

[27] D. Taylor, Geometrical effects in fatigue: a unifying theoretical model, International Journal of Fatigue 21 (5) (1999) 413 – 420.

[28] H. Neuber, Kerbspannungslehre, Springer-Verlag, 1958.

[29] H. Neuber, ber die bercksichtigung der spannungskonzentration bei festigkeitsberechnungen, Konstruktion 20 (7) (1968) 245–251.

[30] L. Susmel, The theory of critical distances: a review of its applications in fatigue, Engineering Fracture Mechanics 75 (7) (2008) 1706 – 1724.

[31] N. Kawagoishi, Q. Chen, H. Nisitani, Fatigue strength of inconel 718 at elevated temperatures, Fatigue & Fracture of Engineering Materials & Structures 23 (3) 209–216.